LETTER

nature cell biology

FHOD1 interaction with nesprin-2G mediates TAN line formation and nuclear movement

Stefan Kutscheidt[1,4], Ruijun Zhu[2,4], Susumu Antoku[2,4], G. W. Gant Luxton[2,5], Igor Stagljar[3], Oliver T. Fackler[1,6] and Gregg G. Gundersen[2,6]

Active positioning of the nucleus is integral to division, migration and differentiation of mammalian cells[1]. Fibroblasts polarizing for migration orient their centrosomes by actin-dependent nuclear movement[2]. This nuclear movement depends on nesprin-2 giant (N2G), a large, actin-binding outer nuclear membrane component of transmembrane actin-associated (TAN) lines that couple nuclei to moving actin cables[3]. Here, we identify the diaphanous formin FHOD1 as an interaction partner of N2G. Silencing FHOD1 expression or expression of fragments containing binding sites for N2G or FHOD1 disrupted nuclear movement and centrosome orientation in polarizing fibroblasts. Unexpectedly, silencing of FHOD1 expression did not affect the formation or rearward flow of dorsal actin cables required for nuclear positioning. Rather, N2G–FHOD1 interaction provided a second connection to actin cables essential for TAN line formation and thus nuclear movement. These results reveal a unique function for a formin in coupling an organelle to actin filaments for translocation, and suggest that TAN lines require multi-point attachments to actin cables to resist the large forces necessary to move the nucleus.

Diaphanous-related formins (DRFs) constitute a family of Rho GTPase-regulated proteins that regulate actin and microtubule cytoskeletons, thereby affecting multiple and diverse cellular processes[4,5]. Most DRFs stimulate nucleation and/or elongation of linear actin filaments required for structures such as filopodia, lamellipodia and contractile rings. Despite similar domain organization and sequence homology to other formins, the DRF FHOD1 does not nucleate or elongate actin filaments, but rather bundles them[6]. The bundling activity of FHOD1 requires an actin-binding region in the amino-terminal regulatory domain and dimerization mediated by the FH2 domain[6]. Consistent with the biochemistry, expression of constitutively active FHOD1 (FHOD1 ΔC) lacking the carboxy-terminal autoinhibitory domain in cells induces formation of thick actin cables that are decorated by the formin, another property that distinguishes FHOD1 from other DRFs (refs 7,8). Although recent reports imply that FHOD1 is hijacked during infection by various pathogens[9,10] and contributes to adhesion maturation[11], cellular functions of FHOD1 remain largely unexplored.

RESULTS

As our previous results indicated that the structure and protein interactions of the FHOD1 N terminus are distinct from other DRFs (ref. 12) and this domain is essential for actin cable formation by FHOD1 ΔC (refs 7,13), we sought to identify binding partners of the N-terminal domain. A yeast two-hybrid screen using residues 1–339 of human FHOD1 as bait identified residues 1340–1678 of human N2G as an interaction partner (Fig. 1a). Consistent with this interaction, GST–N2G 1340–1678 but not GST alone pulled down HA-tagged FHOD1 1–339 from HEK293T cell lysates (Fig. 1b). GST–N2G 1340–1678 also bound specifically to HA–FHOD1 wild type (WT) and HA–FHOD1 ΔC (residues 1–1109). Importantly, HA–FHOD1 WT also immunoprecipitated with full-length endogenous N2G (Fig. 1c).

To further map the FHOD1-binding site in N2G, fragments spanning the length of mouse N2G were tested by yeast two-hybrid screening for interaction with FHOD1 1–339. This mapping revealed that fragment H (residues 1130–1724) encompassing the region identified in the original yeast two-hybrid screen was the only region of N2G that interacted with FHOD1 1–339 (Fig. 1d). Fragments containing the C terminus of FHOD1 did not interact with the H fragment or adjacent I or J fragments, the latter of which contains the N2G actin-binding calponin homology (CH) domains (Supplementary Fig. 1a–c). An N2G H fragment efficiently

[1]Department of Infectious Diseases, Integrative Virology, University Hospital Heidelberg, Heidelberg, INF 324, 69120 Heidelberg, Germany. [2]Department of Pathology and Cell Biology, Columbia University, New York, New York 10032, USA. [3]Department of Molecular Genetics, University of Toronto, Toronto, Ontario M5S 3E1, Canada. [4]These authors contributed equally to this work. [5]Present address: Department of Biology, University of Minnesota, Minneapolis, Minnesota 55455, USA. [6]Correspondence should be addressed to O.T.F. or G.G.G. (e-mail: oliver.fackler@med.uni-heidelberg.de or ggg1@columbia.edu)

Received 18 December 2013; accepted 30 April 2014; published online 1 June 2014; DOI: 10.1038/ncb2981; corrected online 6 June 2014

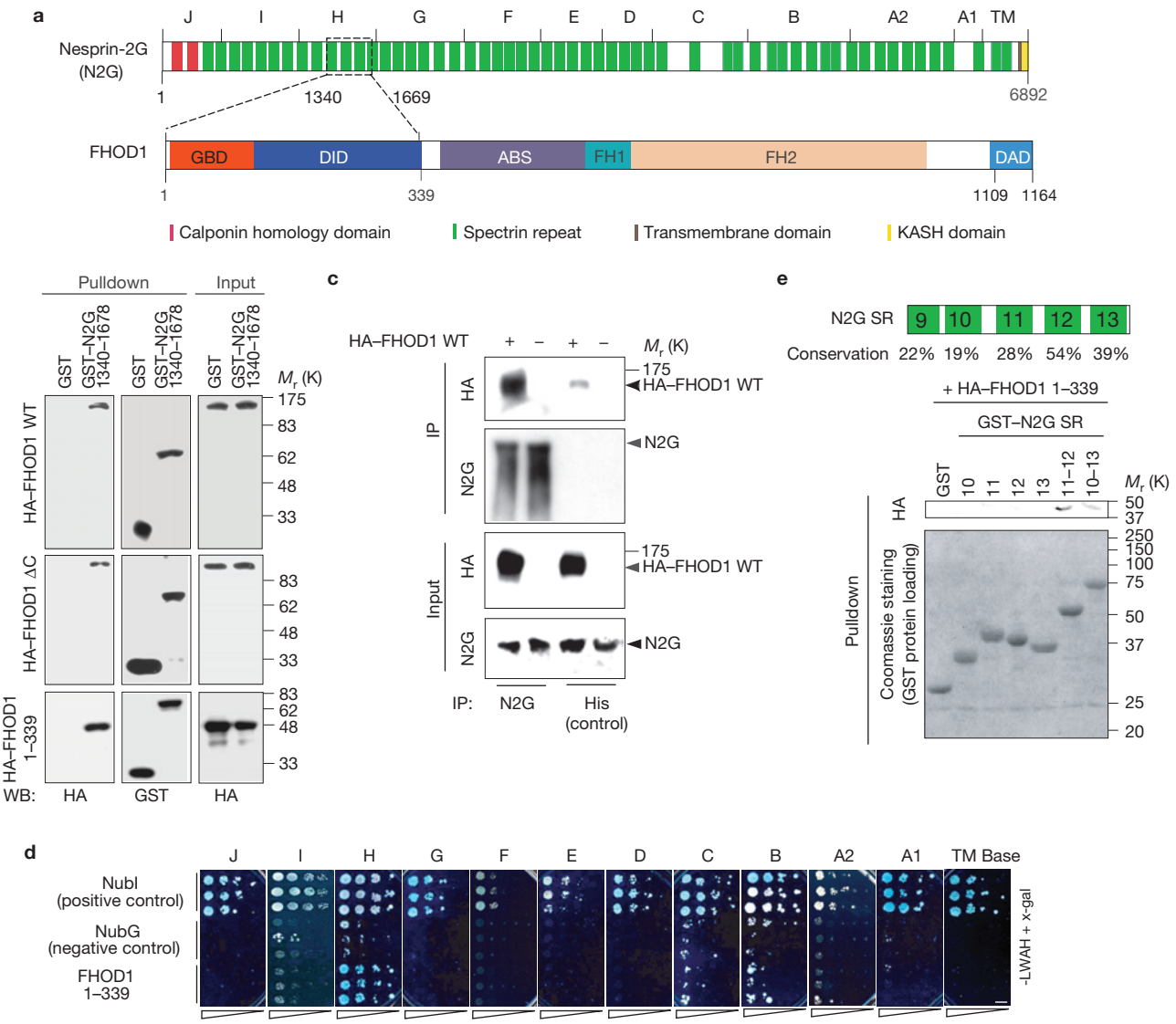

Figure 1 FHOD1 interacts with N2G. (**a**) Schematic representation of the interaction site between human FHOD1 and N2G identified by yeast two-hybrid screening is shown mapped onto mouse N2G and is indicated by the dashed rectangle. The letters above N2G refer to fragments used for the directed yeast two-hybrid screen in **d**. Domains in FHOD1 are: GBD, GTPase binding domain; DID, diaphanous inhibitory domain; ABS, actin-binding site; FH1, formin homology 1 domain; FH2, formin homology 2 domain; DAD, diaphanous autoregulatory domain. (**b**) Pulldown of HA–FHOD1 constructs with GST–N2G 1340–1678. HEK293T cell lysates containing the indicated HA–FHOD1 constructs were pulled down with GST–N2G 1340–1678 or GST and analysed by western blotting (WB) with HA or GST antibody. (**c**) Co-immunoprecipitation (IP) of HA–FHOD1 WT with antibody against endogenous N2G (or unrelated His antibody as a control) from lysates of transfected 293T cells. Immunoprecipitates were analysed by western blotting with antibodies against HA and N2G. (**d**) Directed membrane yeast two-hybrid screen with the indicated N2G fragments as baits and FHOD1 1–339 as prey and positive and negative controls. Triplicates at increasing dilution are shown. Only fragment H interacted above the background level with FHOD1 1–339. Scale bar, 5 mm. (**e**) Pulldown of HA–FHOD1 1–339 with indicated SRs from the interacting region of N2G. The evolutionary conservation of the residues in each of the SRs is indicated (see Methods and Supplementary Fig. 1). Lysates from 293T cells expressing HA–FHOD1 1–339 were pulled down with the indicated GST-tagged N2G SR constructs or GST alone and analysed by western blotting with an antibody against HA. Coomassie staining is shown for GST loads. Uncropped images of blots are shown in Supplementary Fig. 6.

co-immunoprecipitated with HA–FHOD1 WT when coexpressed in 293T cells (Supplementary Fig. 1d).

These results identify an association of FHOD1 with N2G mediated by the N terminus of FHOD1 and residues 1340–1678 in N2G. This region of N2G spans three predicted spectrin repeats (SRs 10–12) and part of a fourth (SR13). Interestingly, SRs 11–13 were previously identified as the second most evolutionarily conserved set of spectrin repeats in N2G (refs 14,15). Alignment of these repeats reveals a higher evolutionary conservation (28–54%) than the ~20% conservation that is generally observed between unrelated SRs (refs 14,15; Fig. 1e and Supplementary Fig. 1e). Consistent with a specialized function of the FHOD1-interacting region in N2G, the region is not conserved in nesprin-1G (refs 14,15). To identify specific N2G SRs involved in interaction with the N terminus of FHOD1, we used various GST-tagged fragments of N2G SRs 10–13 to pull down HA–FHOD1 1–339 expressed in HEK293T cells. This analysis showed that fragments of

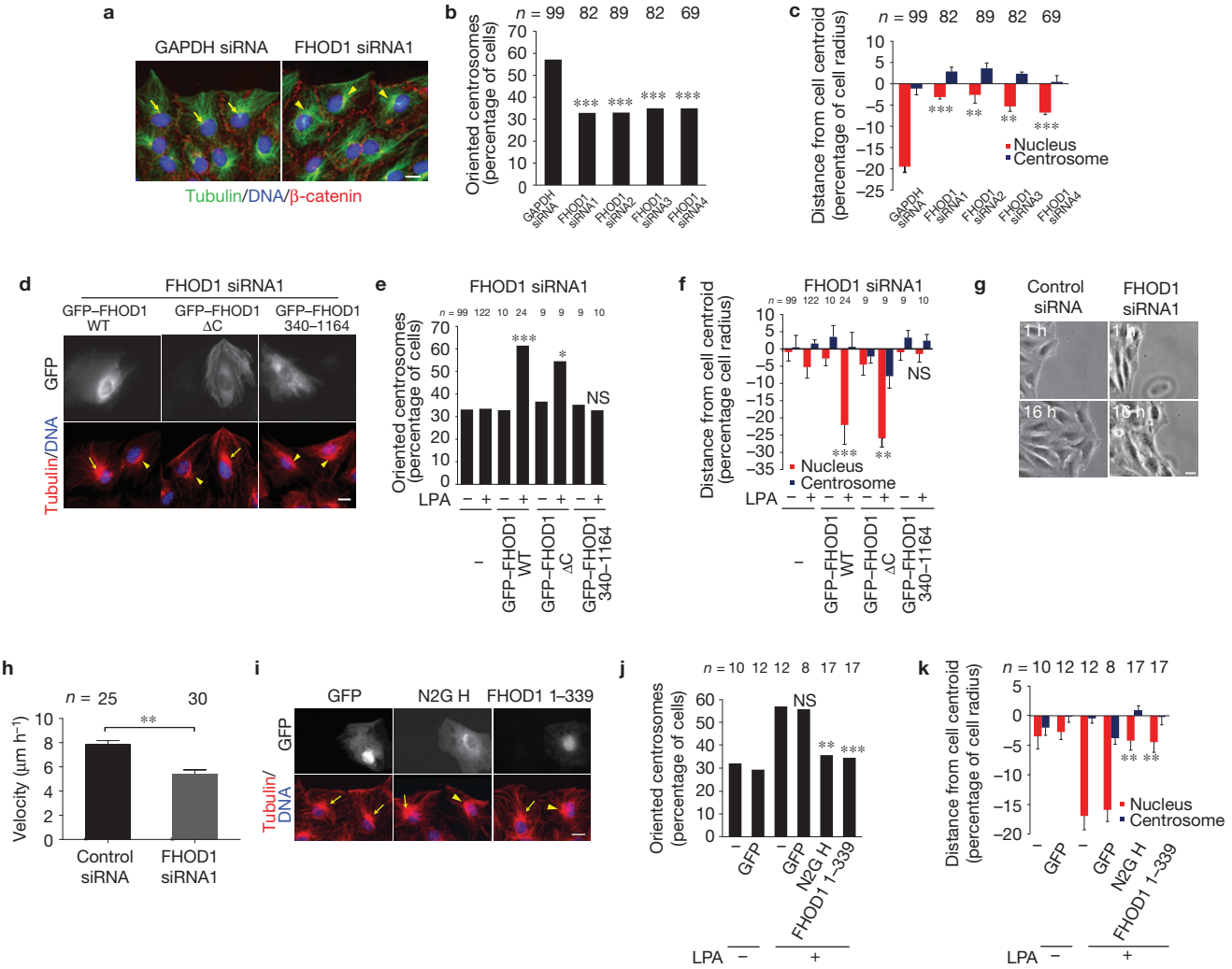

Figure 2 FHOD1 is required for nuclear movement. (**a**) Immunofluorescence images of LPA-stimulated, wounded monolayers of NIH3T3 fibroblasts depleted of GAPDH or FHOD1. The wound is towards the top in this and all subsequent figures. Arrows and arrowheads indicate oriented and non-oriented centrosomes, respectively. (**b**) Quantification of centrosome orientation in the experiment shown in **a**. Centrosome orientation between the leading edge and nucleus was scored as described previously[2,16]; random orientation is 33% by this measure. (**c**) Quantification of centrosome and nucleus position along the front–back axis in LPA-stimulated NIH3T3 fibroblasts depleted of GAPDH or FHOD1. The cell centroid is defined as 0; positive values, towards the leading edge; negative, away. Data in **a**–**c** are from 3 experiments; *n*, number of cells analysed per experiment in this and subsequent panels. (**d**) Immunofluorescence images of LPA-stimulated, wounded monolayers of FHOD1-siRNA1-treated NIH3T3 fibroblasts re-expressing the indicated FHOD1 constructs. Arrows indicate oriented centrosomes; arrowheads, non-oriented centrosomes. (**e**) Quantification of centrosome orientation in the experiment shown in **d**. (**f**) Analysis of centrosome and nucleus position in the experiment shown in **d**. Data in **d**–**f** are from 3 experiments. (**g**) Images from a phase-contrast movie of NIH3T3 fibroblast migrating into wounds after treatment with FHOD1 siRNA1 or scrambled control siRNA. The dashed line shows the wound edge. (**h**) Velocity of wound closure in NIH3T3 fibroblasts treated with FHOD1 siRNA1 or scrambled control siRNA. Data are from 3 individual experiments. (**i**) Immunofluorescence images of LPA-stimulated, wounded monolayers of NIH3T3 fibroblasts expressing interacting regions of N2G or FHOD1. Arrows indicate oriented centrosomes; arrowheads, non-oriented centrosomes. (**j**) Quantification of centrosome orientation in the experiment shown in **i**. (**k**) Analysis of centrosome and nucleus position in the experiment shown in **i**. Data in **i**–**k** are from 4 experiments. Scale bars, **a**,**d**,**g**,**i**: 10 μm. Error bars for **c**,**f**,**h**,**k**: s.e.m. The number (*n*) of cells analysed is shown in **b**,**c**,**e**,**f**,**h**,**j**,**k** $^{***}P < 0.001$; $^{**}P < 0.01$; $^{*}P < 0.05$; NS, not significantly different by Fisher's exact test (**b**,**e**,**j**) and two-tailed *t*-test (**c**,**f**,**h**,**k**).

N2G containing SRs 11–12 associated with FHOD1 1–339, whereas individual SRs did not associate (Fig. 1e). This identifies SRs 11–12 of N2G as the interaction site for FHOD1.

N2G is an outer nuclear membrane protein with a relative molecular mass of ~800K essential for nuclear movement and thus centrosome orientation in migrating fibroblasts[3]. In contrast to many nuclear movements that are dependent on microtubules, N2G mediates actin-dependent nuclear movement in starved fibroblasts stimulated by lysophosphatidic acid (LPA) or serum. We examined whether FHOD1 participated in N2G functions in nuclear movement and centrosome orientation by reducing its expression in NIH3T3 fibroblasts with four different short interfering RNAs (siRNAs) (Supplementary Fig. 2). As expected, ~60% of cells treated with control siRNA (to GAPDH) exhibited LPA-stimulated centrosome orientation towards the wound edge[3,16] (Fig. 2a,b). In contrast, reduction of FHOD1 expression by each of the four siRNAs

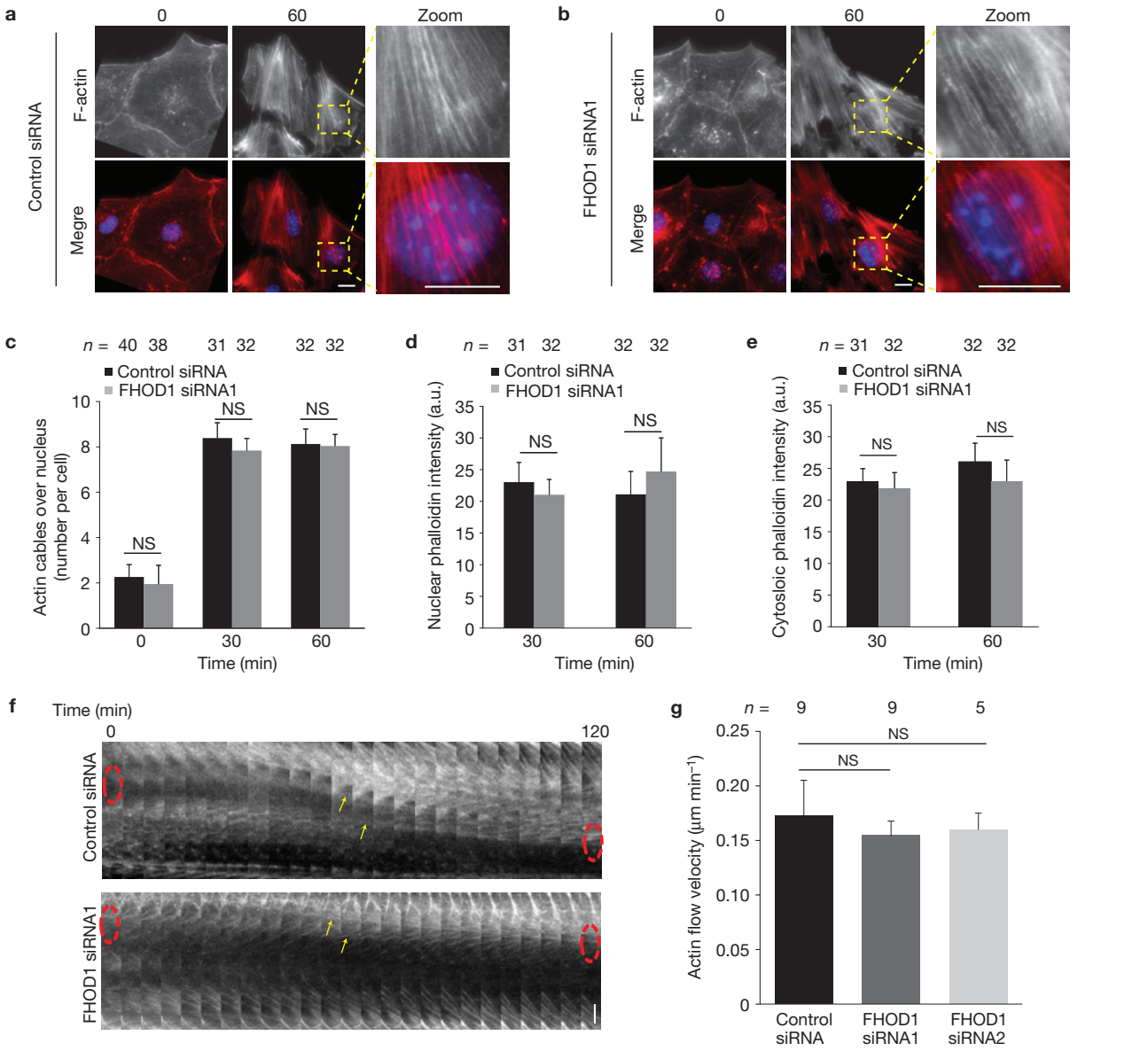

Figure 3 FHOD1 is dispensable for formation of dorsal actin cables and retrograde actin flow. (**a**,**b**) Fluorescence images of F-actin (phalloidin) and DNA (DAPI) in LPA-stimulated NIH3T3 fibroblasts treated with control (**a**) or FHOD1 siRNAs (**b**). Time in min after LPA stimulation is shown at the top. Zoomed images of the outlined regions in the 60 min time point show dorsal actin cables over the nucleus. (**c**–**e**) Quantification of the number of dorsal actin cables above nuclei (**c**), nuclear phalloidin intensity (**d**) and cytosolic phalloidin intensity (**e**) in NIH3T3 fibroblasts treated with control or FHOD1 siRNAs and stimulated with LPA for the indicated time. Data in **a**–**e** are from 5 experiments; *n*, number of cells analysed per experiment in these and subsequent panels. (**f**) Kymographs from movies of Lifeact–GFP stably expressed in NIH3T3 fibroblasts treated with control or FHOD1-specific siRNA. Time (min) is shown above the kymograph; each panel is 5 min. Arrows, retrogradely moving dorsal actin cables; dashed ovals, position of nucleus. (**g**) Velocity of actin cable retrograde flow in NIH3T3 fibroblasts treated with control or FHOD1 siRNAs determined from kymographs as in **f**. Data are from 3 experiments. Scale bars, **a**,**b**: 10 μm; **f**, 5 μm. Error bars, **c**–**e**,**g**: s.e.m. The number (*n*) of cells analysed is shown in **c**–**e**,**g**. NS, not significantly different by two-tailed *t*-test.

reduced centrosome orientation to about 35%, the level observed in unstimulated cells[17]. LPA-stimulated centrosome orientation results from active actin-dependent rearward movement of the nucleus whereas microtubules maintain the centrosome at the cell centroid[2,16]. Analysis of nuclear and centrosome positions revealed that FHOD1 depletion blocked rearward nuclear positioning without affecting the position of the centrosome (Fig. 2c). Centrosome orientation and nuclear movement in FHOD1-depleted cells were rescued by re-expression of full-length FHOD1 WT or constitutively active FHOD1 ΔC, but not by FHOD1 340–1164 lacking the N2G-interacting region (Fig. 2d–f). Consistent with the critical role of nuclear positioning for fibroblast wound closure, migration of NIH3T3 cells into wounds was significantly reduced following FHOD1 depletion (Fig. 2g,h). These results indicate that FHOD1 is required for actin-dependent nuclear movement and suggest that its interaction with N2G is important for this function.

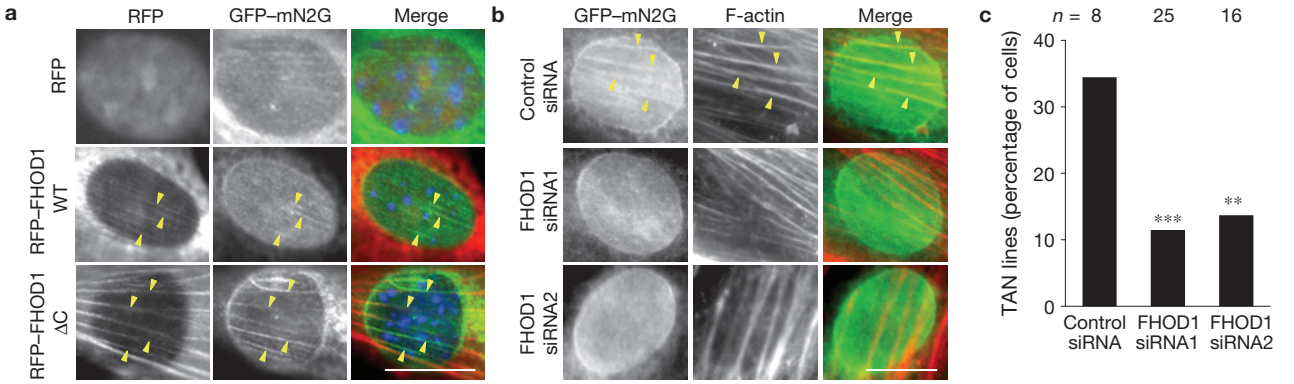

Figure 4 FHOD1 is essential for TAN line formation. (**a**) Fluorescence images of the indicated RFP–FHOD1 constructs or RFP as a control and GFP–mN2G (a TAN line marker) on the dorsal surface of wound edge NIH3T3 fibroblasts. Arrowheads indicate FHOD1 co-localizing with mN2G in TAN lines. (**b**) Fluorescence images of GFP–mN2G and F-actin (phalloidin) on the dorsal surface of wound edge NIH3T3 fibroblasts treated with control or FHOD1 siRNA. Arrowheads, TAN lines with co-localized GFP–mN2G and F-actin. (**c**) Quantification of the frequency of wound-edge NIH3T3 fibroblasts with TAN lines following treatment with the indicated siRNAs. Data are from 3 experiments; *n*, number of cells analysed per experiment in **c**. Scale bars, **a**,**b**: 10 μm. In **c**, $^{***}P < 0.001$; $^{**}P < 0.01$ by Fisher's exact test.

To investigate directly whether FHOD1–N2G interaction was required for centrosome orientation and nuclear movement, we expressed the interacting regions of FHOD1 or N2G in starved NIH3T3 fibroblasts before stimulating them with LPA. Importantly, expression of the N2G H fragment containing SRs 11–12 that interact with FHOD1 potently disrupted LPA-stimulated centrosome orientation and rearward nuclear positioning (Fig. 2i–k). Similarly, FHOD1 1–339, which interacts with N2G and localizes to the nucleus and the cytoplasm[12], also acted as a dominant negative of these processes (Fig. 2i–k). We conclude that the interaction of FHOD1 with N2G is essential for centrosome orientation and rearward nuclear movement.

In NIH3T3 fibroblasts, actin-dependent nuclear movement is mediated by the assembly of N2G-containing TAN lines that couple the nucleus to dorsal actin cables[3]. As reported[3], LPA-stimulated NIH3T3 fibroblasts treated with scrambled siRNA rapidly developed dorsal actin cables over the nucleus (Fig. 3a,c). Despite prevention of centrosome orientation and nuclear movement (Fig. 2b,c), FHOD1 depletion did not affect LPA-induced dorsal actin cables as measured by their numbers over the nucleus or the total intensity of nuclear or cytoplasmic phalloidin fluorescence (Fig. 3b–e). Normal formation of dorsal actin cables was also observed in FHOD1-depleted cells stimulated with serum, even though serum failed to stimulate centrosome orientation in these cells (Supplementary Fig. 3). Importantly, LPA-stimulated retrograde actin cable flow, which drives nuclear movement[2,3], was unaffected by depletion of FHOD1 (Fig. 3f,g). FHOD1 is thus not essential for dorsal actin cable formation or retrograde flow during nuclear movement.

Nuclear movement in NIH3T3 fibroblasts depends on the assembly of N2G along dorsal actin cables to form TAN lines that couple the nucleus to moving actin cables. To test for a potential role of FHOD1 in TAN line formation, we investigated whether FHOD1 localized to these structures. As antibodies for localizing FHOD1 under conditions that preserve TAN lines were unavailable, we localized expressed RFP–FHOD1 constructs. Simultaneous visualization of N2G TAN lines by expression of GFP–mini-N2G (GFP–mN2G) or anti-N2G antibody staining in cells expressing RFP–FHOD1 WT or ΔC revealed that FHOD1 was associated with dorsal actin cables and co-localized with TAN lines (Fig. 4a and Supplementary Fig. 4a). Importantly, in cells depleted of FHOD1, TAN line formation was strongly suppressed as assessed by either expressing GFP–mN2G or staining endogenous N2G, even though dorsal actin cables were evident over the nucleus (Fig. 4b,c and Supplementary Fig. 4b,c). These results indicate that FHOD1 is a component of TAN lines required for their formation.

FHOD1 has two actin-interacting domains: one in its FH2 domain that seems to bind actin barbed ends and one in its N terminus (residues 340–569), termed the N-terminal actin-binding site (ABS), that is required for FHOD1 to decorate actin cables[6,8]. As FHOD1 1–339 containing the N2G-binding site but lacking the N-terminal ABS inhibited nuclear positioning and centrosome orientation (Fig. 2g–i), we investigated the requirement of the N-terminal ABS for FHOD1 function in nuclear positioning by expressing FHOD1 1–569, which contains the N2G-interacting site and the N-terminal ABS (Fig. 5a), in FHOD1-depleted cells. FHOD1 1–569 completely rescued centrosome orientation and partially rescued rearward nuclear positioning (Fig. 5b–d). These results were surprising because they suggested that the FH2 domain of the formin was not absolutely required for rearward nuclear movement. To investigate this further, we prepared a chimaeric construct (NCH, Fig. 5a) composed of the N2G-interacting site in FHOD1 (1–339) and the well-characterized, actin-binding CH domains of α-actinin. Strikingly, NCH rescued centrosome orientation completely and rearward nuclear positioning partially when expressed in FHOD1-depleted cells (Fig. 5b–d). No rescue of these parameters was observed in FHOD1-silenced cells expressing the CH domains of α-actinin alone (Fig. 5a–d). Critically, both FHOD1 1–569 and the NCH chimaera co-localized with dorsal actin cables above the nucleus (Fig. 5e). Coupled with our earlier results that the N2G-binding fragment of FHOD1 (1–339) alone acted as a dominant negative (Fig. 2i–k), these results establish that the

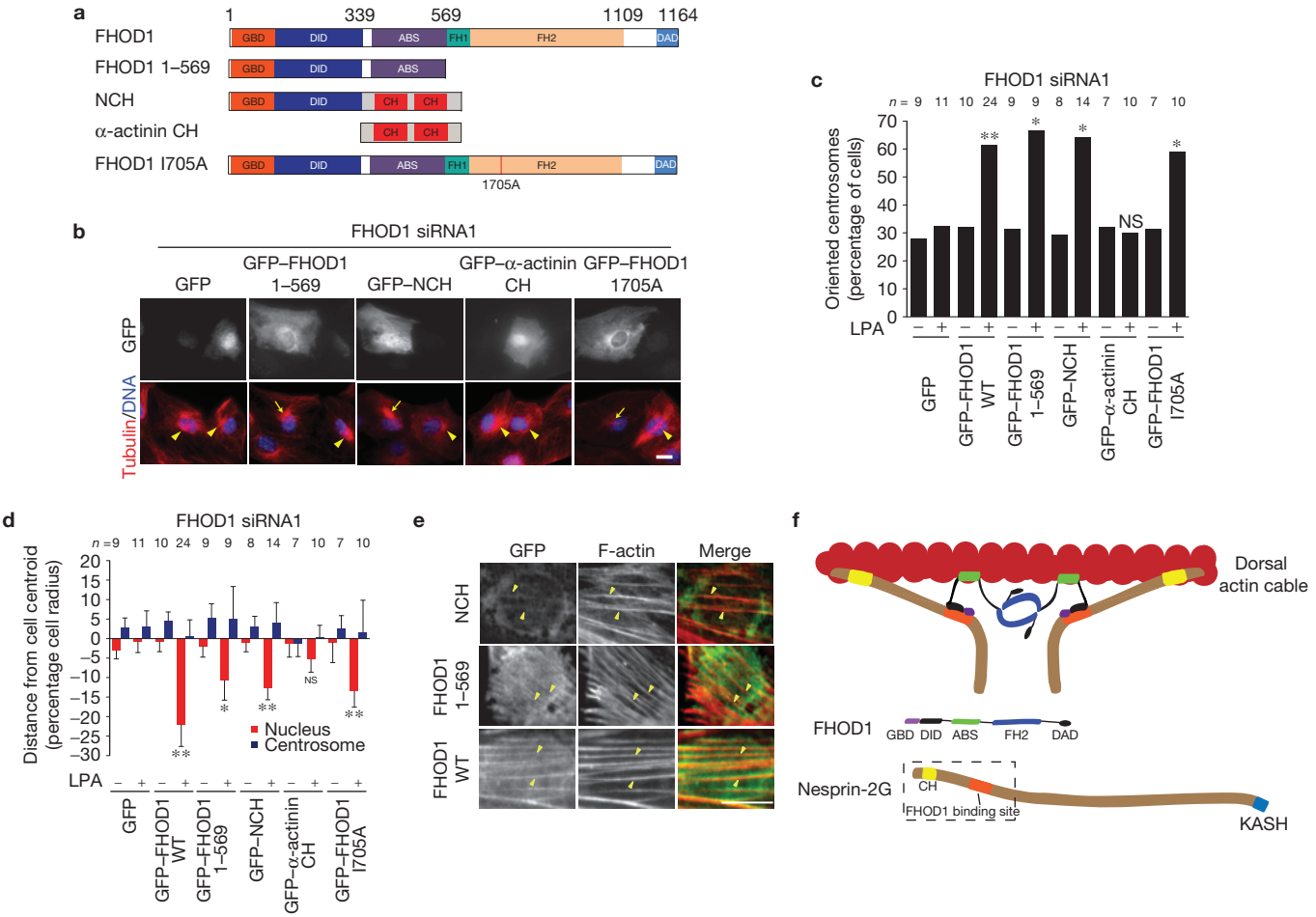

Figure 5 The N-terminal actin-binding site of FHOD1 provides N2G with an additional contact to actin filaments required for TAN line formation. (**a**) Schematic of constructs used. (**b**) Immunofluorescence images of LPA-stimulated, wounded monolayers of FHOD1-siRNA1-treated NIH3T3 fibroblasts expressing the indicated constructs and stained for GFP, Tyr tubulin and DNA (DAPI). Arrows indicate oriented centrosomes; arrowheads, non-oriented centrosomes. (**c**) Quantification of centrosome orientation in the experiment shown in **b**. (**d**) Analysis of centrosome and nucleus position in the experiment shown in **b**. Data in **b**–**d** are from 3 experiments; *n*, number of cells analysed per experiment. (**e**) Immunofluorescence images of the indicated GFP constructs and F-actin (phalloidin) over nuclei of wound-edge NIH3T3 fibroblasts depleted of FHOD1. Arrowheads, examples of expressed GFP protein co-localizing with dorsal actin cables over the nucleus. (**f**) Model of multivalent connection of N2G to actin filaments established by FHOD1–N2G interaction. The paired CH domains of N2G provide one connection to the actin filament; FHOD1 associated with N2G provides a second actin-filament-binding site through its N-terminal ABS. FHOD1 is enlarged relative to N2G to allow depiction of its domains. Scale bars, **b**,**e**: 10 μm. Error bars **d**: s.e.m. $^{**}P < 0.01$; $^{*}P < 0.05$; The number (*n*) of cells analysed is shown in **c**,**d**. NS, not significantly different by Fisher's exact test (**c**) and two-tailed *t*-test (**d**).

N-terminal N2G-interacting site and ABS is the minimal domain of FHOD1 required for centrosome orientation and rearward nuclear positioning.

It was surprising that the FH2 domain, which defines formins, seemed dispensable for centrosome orientation and nuclear positioning. Yet, both FHOD1 1–569 and the chimaera NCH did not fully rescue nuclear positioning. To determine whether the FH2 domain might contribute to this function, we expressed in FHOD1-depleted cells a full-length FHOD1 construct containing a point mutant (FHOD1 I705A, Fig. 5a) in a conserved residue in the FH2 domain that governs actin activity by DRFs (ref. 18). In constitutively active FHOD1 ΔC, the I705A mutation prevented the normal stimulation of actin cable assembly of the WT protein (Supplementary Fig. 5; also see refs 9,10). FHOD1 I705A rescued centrosome orientation but only partially restored rearward nuclear positioning (Fig. 5b–d), suggesting that for full rearward nuclear positioning, both the N-terminal ABS and the FH2 domain are required.

DISCUSSION

The previous model for TAN lines[3,19] proposed that the nucleus and the overlying dorsal actin cables are solely connected by the CH domains of N2G. Our present data suggest that the soluble, cytoplasmic protein FHOD1 plays an essential role in linking the outer nuclear membrane protein N2G to actin cables (Fig. 5f). This model posits that FHOD1 enhances the interaction between N2G and the actin cable by providing N2G with a second physical link to actin. One end of FHOD1 (residues 1–339) connects to N2G

by binding to SRs 11–12 that are unique to N2G; the other end of the N terminus of FHOD1 (residues 340–569) interacts with the actin cable through its ABS (residues ~400–570; refs 6,8). We propose that the N-terminal ABS is critical for forming TAN lines as constructs lacking this site did not rescue FHOD1 depletion and a FHOD1 construct containing only the N2G-binding site was dominant negative for nuclear movement. In addition, a FHOD1 construct that contained both the N2G-interaction site and the N-terminal ABS fully rescued centrosome orientation and largely rescued nuclear movement, as did a chimaeric construct containing the N2G-interacting domain of FHOD1 and the CH domains from α-actinin.

Our model has implications for how N2G connects to dorsal actin cables during nuclear movement. We previously showed that the actin-binding ability of the CH domains of N2G was essential for TAN line formation[3]. Our present data stress that the actin-binding capability of FHOD1 is also necessary for N2G to form TAN lines and move the nucleus. This implies that a multivalent connection between the nesprin and the actin cable is required to resist the force generated by moving such a large organelle as the nucleus. Such a role for FHOD1 may be analogous to that played by the numerous actin-binding proteins that mediate connections between membrane integrin receptors in focal adhesions and actin filaments in stress fibres[20,21]. In addition, the association of FHOD1 with N2G puts its N-terminal ABS in proximity to the CH domains of N2G and this should increase the avidity of N2G interaction with actin filaments and enhance capture of actin cables as they move over the nucleus. Finally, connecting N2G to actin cables through FHOD1 may allow regulation as interactions of the FHOD1 N terminus with its C-terminal autoinhibitory domain or activated GTPases could affect FHOD1–N2G interactions.

The multivalent feature of the model seems at odds with the rescue of TAN line formation and nuclear movement in N2G-depleted cells by mN2G, which lacks the FHOD1-interacting site but contains CH domains[3]. However, because mN2G was overexpressed in these rescue studies, the high levels of CH domains available for interacting with actin cables probably compensate for the multivalent attachment through a single N2G.

A detailed structure of N2G and FHOD1 in association with actin filaments awaits higher-resolution studies. Nonetheless, the extended structure of SR proteins and the conserved 5 nm length of SR repeats makes a prediction about the geometry of N2G relative to the actin filament when it is bound through its CH domains and the N-terminal ABS of FHOD1. The CH domains and the FHOD1-interacting region (SRs 11–12) in N2G would be expected to be separated by as much as 50 nm. Given that the N2G-interacting site and the ABS in the N terminus of FHOD1 probably span less than 10 nm (ref. 12), this predicts that N2G bound to actin through its CH domains and FHOD1 will lie nearly parallel to the long axis of the actin filament (as depicted in Fig. 5f) rather than perpendicular as predicted in earlier models of N2G interaction with actin filaments[1,22].

The involvement of FHOD1 in moving nuclei is a unique function for a formin. Most formins stimulate actin filament elongation by processively binding the barbed end of the actin filament through their FH2 domain. Although the FH2 domain of FHOD1 is highly conserved compared with other DRFs and behaves as if it binds to actin barbed ends, it does not seem to stimulate actin polymerization *in vitro* or in cells[6]. Instead, the main biochemical activity of FHOD1 is in bundling actin filaments and binding along their length and these activities require the unique N-terminal ABS (refs 6,8). The FH2 domain of FHOD1 contributes to bundling by establishing the dimeric nature of FHOD1. Our results suggest that the FH2 domain of FHOD1 may not contribute directly to its activity in TAN line formation. Yet, the lack of complete rescue of nuclear movement with FHOD1 constructs bearing FH2 domain mutations or deletions suggests that it may contribute, perhaps by promoting dimerization to additionally stabilize TAN line structure by crosslinking adjacent nesprins.

FHOD1 function in nuclear movement resembles that recently described for the formin INF2 in binding endoplasmic reticulum membranes and contributing to their scission by deforming them in an actin-dependent fashion[23]. There are 15 formin family members in mammals and it will be interesting to investigate whether other members of this family also function as proteins that mediate force transmission between the actin cytoskeleton and membranes. □

METHODS

Methods and any associated references are available in the online version of the paper.

Note: Supplementary Information is available in the online version of the paper

ACKNOWLEDGEMENTS

We thank D. Discher and M. Geyer for helpful discussion. This work was financially supported in part by the Deutsche Forschungsgemeinschaft (GRK1188 to S.K., grant FA 378/6-2 to O.T.F.) and NIH (grant GM099481 to G.G.G.). O.T.F. is a member of the CellNetworks Cluster of Excellence EXC81.

AUTHOR CONTRIBUTIONS

G.G.G. and O.T.F. conceived the study, designed experiments and wrote the manuscript. S.K., R.Z., S.A., G.W.L. and I.S. designed and conducted experiments and discussed and interpreted the data together with O.T.F. and G.G.G.

COMPETING FINANCIAL INTERESTS

The authors declare no competing financial interests.

Published online at www.nature.com/doifinder/10.1038/ncb2981
Reprints and permissions information is available online at www.nature.com/reprints

1. Gundersen, G. G. & Worman, H. J. Nuclear positioning. *Cell* **152,** 1376–1389 (2013).
2. Gomes, E. R., Jani, S. & Gundersen, G. G. Nuclear movement regulated by Cdc42, MRCK, myosin, and actin flow establishes MTOC polarization in migrating cells. *Cell* **121,** 451–463 (2005).
3. Luxton, G. W., Gomes, E. R., Folker, E. S., Vintinner, E. & Gundersen, G. G. Linear arrays of nuclear envelope proteins harness retrograde actin flow for nuclear movement. *Science* **329,** 956–959 (2010).
4. Chesarone, M. A., DuPage, A. G. & Goode, B. L. Unleashing formins to remodel the actin and microtubule cytoskeletons. *Nat. Rev. Mol. Cell Biol.* **11,** 62–74 (2010).
5. Bartolini, F. & Gundersen, G. G. Formins and microtubules. *Biochim. Biophys. Acta* **1803,** 164–173 (2010).
6. Schonichen, A. *et al.* FHOD1 is a combined actin filament capping and bundling factor that selectively associates with actin arcs and stress fibers. *J. Cell Sci.* **126,** 1891–1901 (2013).
7. Gasteier, J. E. *et al.* Activation of the Rac-binding partner FHOD1 induces actin stress fibers via a ROCK-dependent mechanism. *J. Biol. Chem.* **278,** 38902–38912 (2003).
8. Takeya, R. & Sumimoto, H. Fhos, a mammalian formin, directly binds to F-actin via a region N-terminal to the FH1 domain and forms a homotypic complex via the FH2 domain to promote actin fiber formation. *J. Cell Sci.* **116,** 4567–4575 (2003).

9. Alvarez, D. E. & Agaisse, H. The formin FHOD1 and the small GTPase Rac1 promote vaccinia virus actin-based motility. *J. Cell Biol.* **202,** 1075–1090 (2013).
10. Truong, D. *et al.* Formin-mediated actin polymerization promotes Salmonella invasion. *Cell. Microbiol.* **15,** 2051–2063 (2013).
11. Iskratsch, T. *et al.* FHOD1 is needed for directed forces and adhesion maturation during cell spreading and migration. *Dev. Cell* **27,** 545–559 (2013).
12. Schulte, A. *et al.* The human formin FHOD1 contains a bipartite structure of FH3 and GTPase-binding domains required for activation. *Structure* **16,** 1313–1323 (2008).
13. Koka, S. *et al.* The formin-homology-domain-containing protein FHOD1 enhances cell migration. *J. Cell Sci.* **116,** 1745–1755 (2003).
14. Simpson, J. G. & Roberts, R. G. Patterns of evolutionary conservation in the nesprin genes highlight probable functionally important protein domains and isoforms. *Biochem. Soc. Trans.* **36,** 1359–1367 (2008).
15. Autore, F. *et al.* Large-scale modelling of the divergent spectrin repeats in nesprins: giant modular proteins. *PLoS ONE* **8,** e63633 (2013).
16. Schmoranzer, J. *et al.* Par3 and dynein associate to regulate local microtubule dynamics and centrosome orientation during migration. *Curr. Biol.* **19,** 1065–1074 (2009).
17. Palazzo, A. F., Cook, T. A., Alberts, A. S. & Gundersen, G. G. mDia mediates Rho-regulated formation and orientation of stable microtubules. *Nat. Cell Biol.* **3,** 723–729 (2001).
18. Bartolini, F. *et al.* The formin mDia2 stabilizes microtubules independently of its actin nucleation activity. *J. Cell Biol.* **181,** 523–536 (2008).
19. Luxton, G. W., Gomes, E. R., Folker, E. S., Worman, H. J. & Gundersen, G. G. TAN lines: a novel nuclear envelope structure involved in nuclear positioning. *Nucleus* **2,** 173–181 (2011).
20. Ciobanasu, C., Faivre, B. & Le Clainche, C. Integrating actin dynamics, mechanotransduction and integrin activation: the multiple functions of actin binding proteins in focal adhesions. *Eur. J. Cell Biol.* **92,** 339–348 (2013).
21. Pellegrin, S. & Mellor, H. Actin stress fibres. *J. Cell Sci.* **120,** 3491–3499 (2007).
22. Starr, D. A. & Fridolfsson, H. N. Interactions between nuclei and the cytoskeleton are mediated by SUN-KASH nuclear-envelope bridges. *Annu. Rev. Cell Dev. Biol.* **26,** 421–444 (2010).
23. Korobova, F., Ramabhadran, V. & Higgs, H. N. An actin-dependent step in mitochondrial fission mediated by the ER-associated formin INF2. *Science* **339,** 464–467 (2013).

DOI: 10.1038/ncb2981

METHODS

Reagents. LPA was from Avanti Polar Lipids. Alexa647–phalloidin was from Invitrogen. 4′,6-diamidino-2-phenylindole dihydrochloride was from LifeTechnologies. Unless noted, all other chemicals were from Sigma-Aldrich. Lifeact–mCherry[24] was from ibidi. HA–FHOD1 expression plasmids (WT, ΔC, 1–339, 1–569) were described earlier[7,25]. GFP–FHOD1 constructs were made by amplifying the corresponding sequences from HA–FHOD1 and insertion into pEGFP–C2 (Clontech) using EcoRI. GFP–FHOD1I705A was made by PCR-based mutagenesis. mRFP–FHOD1 WT and ΔC were made by excising the corresponding FHOD1 sequences with EcoRI from pEGFP–C2 plasmids and inserting into the EcoRI site of EF–pLINK2–FLAG–mRFP (gift from R. Grosse, Marburg). N2G1340-1678 was amplified from HeLa cell cDNA and cloned into pGEX–2TK (GE Healthcare) through the SmaI restriction site. GFP–mN2G was described earlier[3]. mCherry–mN2G was prepared by inserting the mN2G sequence from GFP–mN2G into the SalI and XbaI sites of pmCherry–C1 (Clontech). The GFP–N2G H and HI fragments were prepared by PCR amplifying the corresponding regions from NIH3T3 fibroblast cDNA and inserting into the NotI site of pEGFP–C4. GFP–α-actinin CH (residues 1–269) was made by PCR amplifying it from HeLa cell cDNA and inserting the product into the BamHI and NotI sites of the pEGFP–C4 vector. GFP–NCH was made by fusing α-actinin CH domains to the C terminus of FHOD1 1–339 without a linker and then inserting the chimaera into the BamHI and NotI sites of pEGFP–C4. All constructs were verified by sequencing.

Cell culture. NIH3T3 fibroblasts were cultured in DMEM (Corning Cellgro) plus 10% calf serum (Hyclone or Thermo Fisher Scientific) and serum-starved for 36–48 h as previously described[26]. For centrosome orientation, wounded monolayers of starved NIH3T3 fibroblasts were treated with 10 μM LPA in serum-free DMEM as previously described[17]. For some experiments, cDNAs (25–75 ng μl^{-1}) were microinjected into nuclei of cells at the edge of wounds and allowed to express for 1–2 h before LPA stimulation. HEK293T cells were grown in DMEM (Gibco) with 10% FBS (Hyclone or BiochromAG).

Yeast-two hybrid screening. The initial Y2H screen that identified N2G 1340–1678 as a binding partner of FHOD1 1–339 was performed by Hybrigenics Services. FHOD1 1–339 was cloned into the Y2H bait vectors pB29 (N-bait-LexA-C fusion) and pB43 (N-bait-GAL4-C fusion) and screened against a human leukocyte/activated mononuclear cell RP1 cDNA library. In total, more than 166 million interactions were analysed and yielded 85 putative interacting clones. Among these, 20 in-frame cDNA clones were isolated, of which only N2G was identified using both bait vectors.

The directed interaction screen was done using the membrane yeast two-hybrid system[27] using FHOD1 1–339 as prey and fragments along the length of N2G as bait. Mouse N2G for the baits was PCR amplified from NIH3T3 fibroblast cDNA (see Supplementary Table 1 for sequence differences between the NIH3T3 N2G sequence and that reported for mouse N2G on NCBI). Each N2G fragment was directly fused with the N terminus of a N2G construct containing the C-terminal transmembrane domain (termed TM Base, encoding residues 6551–6892 of mouse N2G) without a linker. These N2G fragments were inserted into yeast expression vectors pBT3–N or pTLB–1 with the following restriction sites (N2G fragment/plasmid/restriction sites): TM base/pBT3–N/NcoI-SacII, A1/pBT3–N/NcoI–SacII, A2/pBT3–N/NcoI–SacII, B/pTLB-1/SacII, C/pTLB-1/SacII, D/pBT3–N/NcoI–SacII, E/pBT3–N/NcoI–SacII, F/pBT3–N/NcoI–SacII, G/pBT3–N/NcoI–SacII, H/pTLB-1/SacII, I/pTLB-1/SacII, and J/pBT3–N/NcoI–SacII. The FHOD1 prey constructs were inserted into the BamHI and EcoRI restriction sites of the pPR3–N vector. Interactions were screened by growth using pOST–NubI and pOST–NubGas positive and negative and controls, respectively.

Co-immunoprecipitation and pulldown. HEK293T cells were transfected with plasmids encoding tagged proteins using polyethylenimine (Sigma-Aldrich) according to the manufacturer's instructions. After 20 h, cells were lysed in 1% Triton X-100, 25 mM Tris-HCl, pH 8.0, 2 mM EDTA, 150 mM NaCl, and protease inhibitor mix (Roche). A small aliquot of the lysate was kept as input sample. The lysate was incubated with rabbit anti-nesprin-2G or mouse anti-HA for 5 h at 4 °C. Antibody complexes were recovered on protein A–Sepharose (GE Healthcare), preblocked with cell lysate from untransfected cells, and then eluted with SDS–PAGE sample buffer with boiling. Immunoprecipitates were run on NuPAGE gradient gel (Invitrogen) (for detection of endogenous N2G) or 10% Tris-glycine SDS–PAGE gels for co-immunoprecipitation with GFP–N2G HI and western blots were developed with the following antibodies: rabbit anti-N2G (1:10,000; ref. 3), mouse anti-HA (1:500, SC-7392, clone F-7, Santa Cruz Biotechnology), rabbit anti-His (1:500, SC-804, Santa Cruz Biotechnology), and mouse anti-GFP (1:2,000, G6539, clone GFP-20, Sigma-Aldrich).

GST–N2G 1340–1678, various GST–N2G spectrin repeats, or GST proteins for pulldowns were expressed in *Escherichia coli* BL21 (DE3) by induction with 1 mM IPTG. Bacteria were spun down and the pellet was resuspended in ice-cold TBS, 10 mM $MgCl_2$, 1 mM dithiothreitol and protease inhibitor mix (Roche). After sonication the bacterial lysate was supplemented with 1% Triton X-100 and incubated on a shaker for 30 min at 4 °C. After centrifugation, the cleared supernatant was incubated with glutathione–Sepharose (GE Healthcare) for 3 h to bind GST or GST-tagged N2G proteins. Following washing, 10% glycerol was added and the Sepharose suspension was aliquoted, quick frozen in liquid nitrogen and stored at −80 °C. For pulldowns, HEK293T cells were transfected with HA-tagged FHOD1 WT, FHOD1 1–339 or FHOD1ΔC using Lipofectamine 2000 (Life Technologies). Cells were lysed in 1% Triton X-100, 25 mM Tris-HCl, pH 8.0, 2 mM EDTA, supplemented with 50 mM NaCl (for HA–FHOD1 1–339) or 100 mM NaCl (for FHOD1 WT and ΔC). After clearing, lysates were incubated for 4 h at 4 °C with GST or GST–N2G 1340–1678 Sepharose that had been preblocked with cell lysate from untransfected cells. After washing with lysis buffer supplemented with 50, 100 or 150 mM NaCl for HA–FHOD1 1–339, FHOD1 WT and HA–FHOD1 ΔC, respectively, bound proteins were eluted with SDS sample buffer, boiled, and analysed by western blotting with mouse anti-GST (1:1,000, SC-138, clone B-14, Santa Cruz Biotechnology) and mouse anti-HA. For pulldown of HA-tagged FHOD1 1–339 with various GST–N2G spectrin repeat constructs, HEK293T cells were transfected with HA-tagged FHOD1 1–339 by calcium phosphate. Two days after transfection, cells were lysed in 1% Triton X-100, 25 mM Tris-HCl, pH 7.4, 150 mM NaCl, 5 mM EDTA, 1 mM Na_3VO_4, 1 mM NaF, 10% glycerol, and protease inhibitor mix (Roche). After clearing, lysates were incubated for 2 h at 4 °C with GST or GST fused with various N2G spectrin repeats immobilized on Sepharose. After washing with the lysis buffer, bound proteins were eluted with SDS sample buffer, boiled, and analysed by Coomassie brilliant blue staining or western blotting with rabbit anti-HA (1:1,000, H6908, Sigma-Aldrich). Western blot membranes of GST-pulldowns and immunoprecipitates were developed with ECL signal enhancer (Thermo Scientific) to enhance the sensitivity of signal detection.

siRNA knockdown. Duplex siRNAs (21 nucleotides in length) were purchased from Shanghai GenePharma. The sequences used for FHOD1 were: FHOD1 siRNA1, 5′-GAGCGGUCCUAGAGCCUUATT-3′; FHOD1 siRNA2, 5′-GGGCGGAAGCCCACGUUAATT-3′; FHOD1 siRNA3, 5′-CCAGUAUUGUGAACAGUAUTT-3′; FHOD1 siRNA4, 5′-UACCAGAGCUACAUCCUUAUU-3′ and that for GAPDH was 5′-AAAGUUGUCAUGGAUGACCTT-3′ as predicted by BIOPREDsi. Non-coding siRNA was used as a control in some experiments. Transfection with Lipofectamine RNAiMAX (Invitrogen) was carried out according to the manufacturer's instructions. Efficiency of protein depletion was determined by western blot analysis of total cell lysates using rabbit anti-FHOD1 antibody at 1:500 (ref. 28).

Immunostaining. Cells on coverslips were fixed with either 4% paraformaldehyde in PBS for 10 min followed by permeabilization with 0.1% Triton X-100 in PBS for 3 min or −20 °C methanol for 5 min. Fixed cells were stained with the following antibodies: rabbit N2G 1:100 (ref. 3), rabbit anti-pericentrin (1:400, PRB-432C, Covance), rat anti-Tyr tubulin (1:40, clone YL1/2 European Collection of Animal Cell Cultures), chicken anti-GFP (1:100, AB16901, EMD Millipore). Rhodamine phalloidin (1:200, A12379, Invitrogen) was used to stain F-actin. Stained cells were mounted in Vectashield (Invitrogen) or Fluoromount-G (Southern Biotech). Images were acquired with either ×40 Planapo (NA1.0) or ×60 Planapo (NA1.4) objectives and a CoolSNAP HQ CCD (charge-coupled device) camera on a Nikon TE300 inverted microscope controlled by Metamorph (Molecular Devices) and processed with ImageJ (NIH) or with ×60 or ×100 Planapo objectives and an Olympus U-CMAP3 camera on an Olympus IX81 microscope controlled by CellM Olympus software.

Centrosome reorientation and nuclear movement assays and data analysis. Centrosome orientation to a position between the nucleus and the leading edge was analysed as previously described using cells immunofluorescently stained for pericentrin, Tyr tubulin and nuclei[29,30]. Nuclear and centrosomal positions were determined from images of cells immunofluorescently stained for the centrosome (pericentrin), cell boundaries (actin or microtubules) and nuclei (DAPI). Images were uploaded into custom software (available on request) that identifies the positions of the nuclear and cell centroids, the centrosome, cell boundaries and the wound direction[31]. Software determinations of cell boundaries were inspected and corrected manually where necessary using the software to adjust computer drawn boundaries. The x and y positions (x, parallel to wound edge; y, perpendicular) of both the nucleus centroid and centrosome were calculated and normalized to the average cell radius calculated by the software. Only the y positions are depicted in the graphs as little movement of the nucleus or centrosomes along the x axis occurred in the experiments reported.

Quantification of dorsal actin cables and F-actin. LPA- and serum-stimulated wound-edge NIH3T3 fibroblasts that had been stained for F-actin

and nuclei were used to assess the effect of siRNA-mediated FHOD1 knockdown on dorsal actin cables above the nucleus and total F-actin in the cytoplasm and associated with the nucleus. Dorsal actin cables above the nucleus were manually counted from single-plane images taken of F-actin and nuclei counting only those actin cables that passed over the nucleus. Total F-actin in the cytoplasm and associated with the nucleus were determined by measurement of rhodamine phalloidin fluorescence in the region of interest using ImageJ.

Time-lapse microscopy and analysis. For retrograde actin cable flow, NIH3T3 fibroblasts stably expressing Lifeact–GFP were grown to confluency on glass coverslip dishes, serum-starved for 48 h and then wounded and transferred to recording media (MEM amino acids, HBSS, 1% penicillin/streptomycin, 25 mM glucose, 4 mM glutamine, 2 μM sodium pyruvate, and 20 mM HEPES, pH 7.4; GIBCO). Cells were stimulated with LPA and then maintained in a TokaiHit chamber at 35 °C on a Nikon Ti microscope. Images at multiple planes were acquired every 5 min using a ×60 Planapo objective (NA 1.49) and an Andor iXon X3 EMCCD camera controlled by NIS software (Nikon). Kymographs were prepared with NIS software and exported to ImageJ to calculate the rate of movement of dorsal actin cables in the leading lamella.

For cell migration, phase-contrast live-cell movies were prepared of multiple fields of wounded monolayers of NIH3T3 fibroblasts and analysed to determine the migration velocity as previously described.

Image processing and statistical analysis. Images of western blots, yeast two-hybrid, immunofluorescence, and phase contrast are representative of results from three or more separate experiments, except for Fig. 1d, and Supplementary Fig. 1d, which were repeated twice. Images were processed for contrast and brightness and assembled into figures using Adobe Illustrator/Photoshop. For quantitative results, statistical analysis was performed on parametric data using unpaired two-tailed *t*-tests and non-parametric data using Fisher's exact test by GraphPad Prism 5 or Excel.

Sequence comparison. Sequence alignments were created by CLC Sequence Viewer software (CLC bio, Qiagen) using the ClustalW algorithm. The conservation score for each position (range; 1–9, lowest to highest) was obtained from the ClustalW2 program (EMBL-EBI). To calculate an overall conservation score for N2G SRs in the FHOD1 interaction region, positions with a conservation score $\geq$ 8 were counted as positive and the percentage of conservation was calculated as the percentage of positive residues to total residues.

24. Riedl, J. *et al.* Lifeact: a versatile marker to visualize F-actin. *Nat. Methods* **5,** 605–607 (2008).
25. Madrid, R. *et al.* Oligomerization of the diaphanous-related formin FHOD1 requires a coiled-coil motif critical for its cytoskeletal and transcriptional activities. *FEBS Lett.* **579,** 441–448 (2005).
26. Cook, T. A., Nagasaki, T. & Gundersen, G. G. Rho guanosine triphosphatase mediates the selective stabilization of microtubules induced by lysophosphatidic acid. *J. Cell Biol.* **141,** 175–185 (1998).
27. Iyer, K. *et al.* Utilizing the split-ubiquitin membrane yeast two-hybrid system to identify protein-protein interactions of integral membrane proteins. *Sci. STKE* **2005,** pl3 (2005).
28. Gasteier, J. E. *et al.* FHOD1 coordinates actin filament and microtubule alignment to mediate cell elongation. *Exp. Cell Res.* **306,** 192–202 (2005).
29. Gomes, E. R. & Gundersen, G. G. Real-time centrosome reorientation during fibroblast migration. *Methods Enzymol.* **406,** 579–592 (2006).
30. Palazzo, A. F. *et al.* Cdc42, dynein, and dynactin regulate MTOC reorientation independent of Rho-regulated microtubule stabilization. *Curr. Biol.* **11,** 1536–1541 (2001).
31. Chang, W., Folker, E. S., Worman, H. J. & Gundersen, G. G. Emerin organizes actin flow for nuclear movement and centrosome orientation in migrating fibroblasts. *Mol. Biol. Cell.* **24,** 3869–3880 (2013).

nature cell biology

DOI: 10.1038/ncb2981

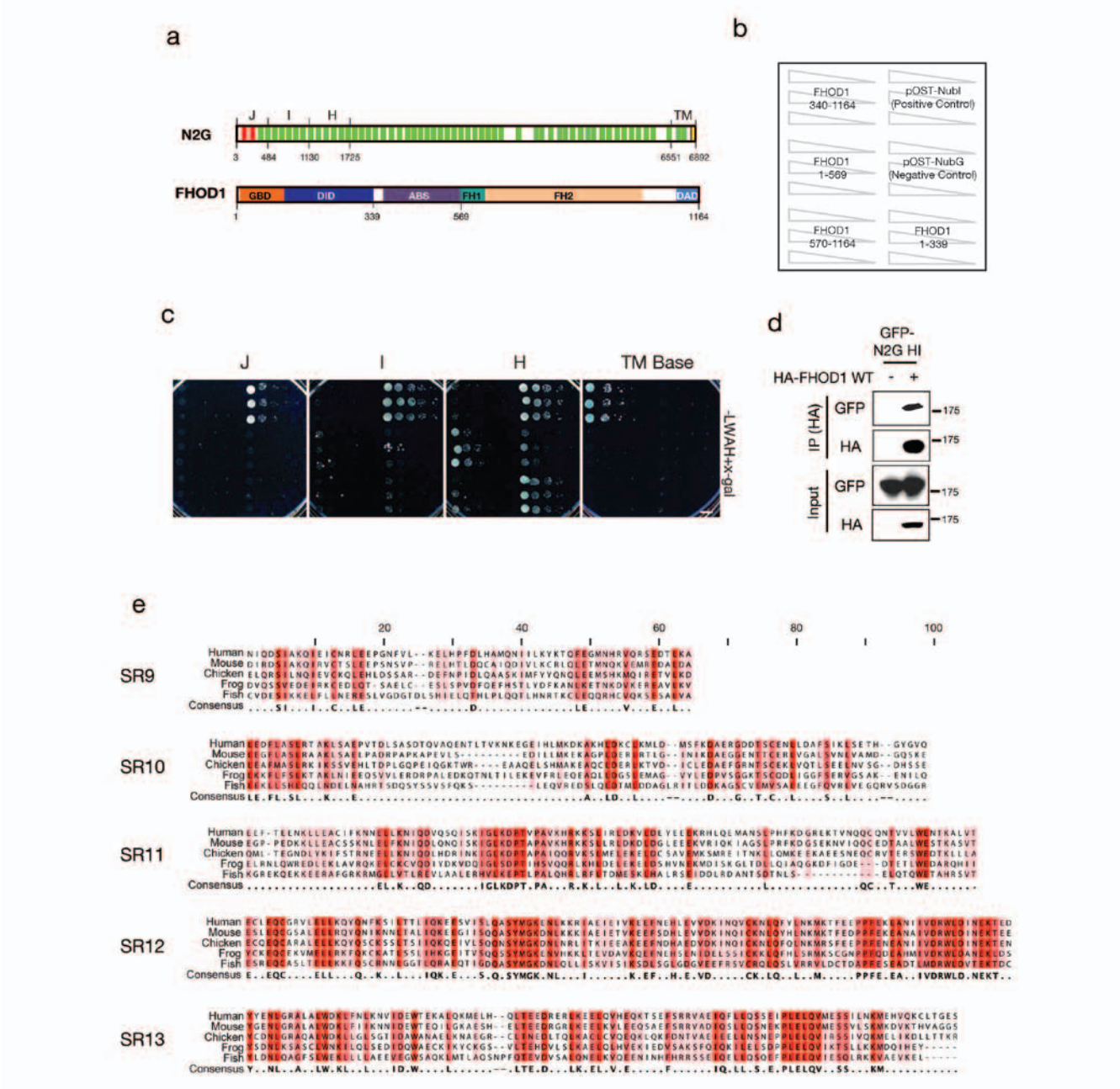

Supplementary Figure 1 Additional evidence that the interaction between FHOD1's N-terminus and nesprin-2G (N2G) is specific and phylogenetic comparison of the FHOD1 interacting region of N2G. (a) Schematic of N2G and FHOD1 with boundaries for constructs used in membrane yeast-two hybrid. (b) Legend for yeast two-hybrid indicating the FHOD1 fragments used as a bait for the experiment shown in panel c. (c) Yeast two-hybrid results for the interaction between N2G J,H and I fragments and FHOD1 fragments indicated in panel b. Bar, 5 mm. (d) N2G HI fragment interacts with HA-FHOD WT in cell lysates. GFP-N2G HI was expressed alone or co-expressed with HA-FHOD1 WT in 293T cells and lysates were immunoprecipitated with HA antibody. Western blots were probed with antibodies for HA and GFP. Input shows level of expression of transfected proteins. (e) Phylogenetic comparison between spectrin repeats (SRs) 9-13 of N2G. Red indicates residues conserved between at least four of the five species; pink indicates residues that are conserved in at least three of the species. Consensus residues are shown below for highly conserved positions. Sequences were obtained from the following sources. Human (*H. sapiens*, NP_878918.2, NCBI), Mouse (*M. musculus*, NIH3T3 fibroblast cDNA), Chicken (*G. gallus*, XP_003641488, NCBI), Frog (*X. tropicanis*, XP_002933763, NCBI), Fish (D. rerio, F1QVC9, Uniport).

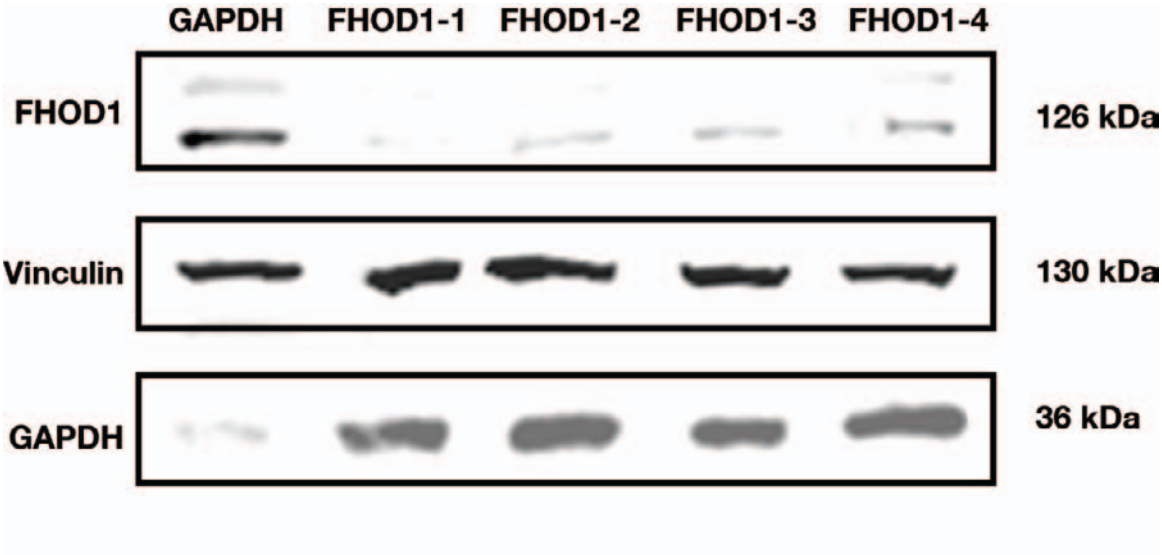

Supplementary Figure 2 FHOD1 knock down by siRNAs. Western blot of FHOD1 levels in NIH3T3 fibroblasts after knockdown with four different siRNAs targeting FHOD1. Control siRNA knockdown of GAPDH is shown for comparison. Vinculin is a loading control.

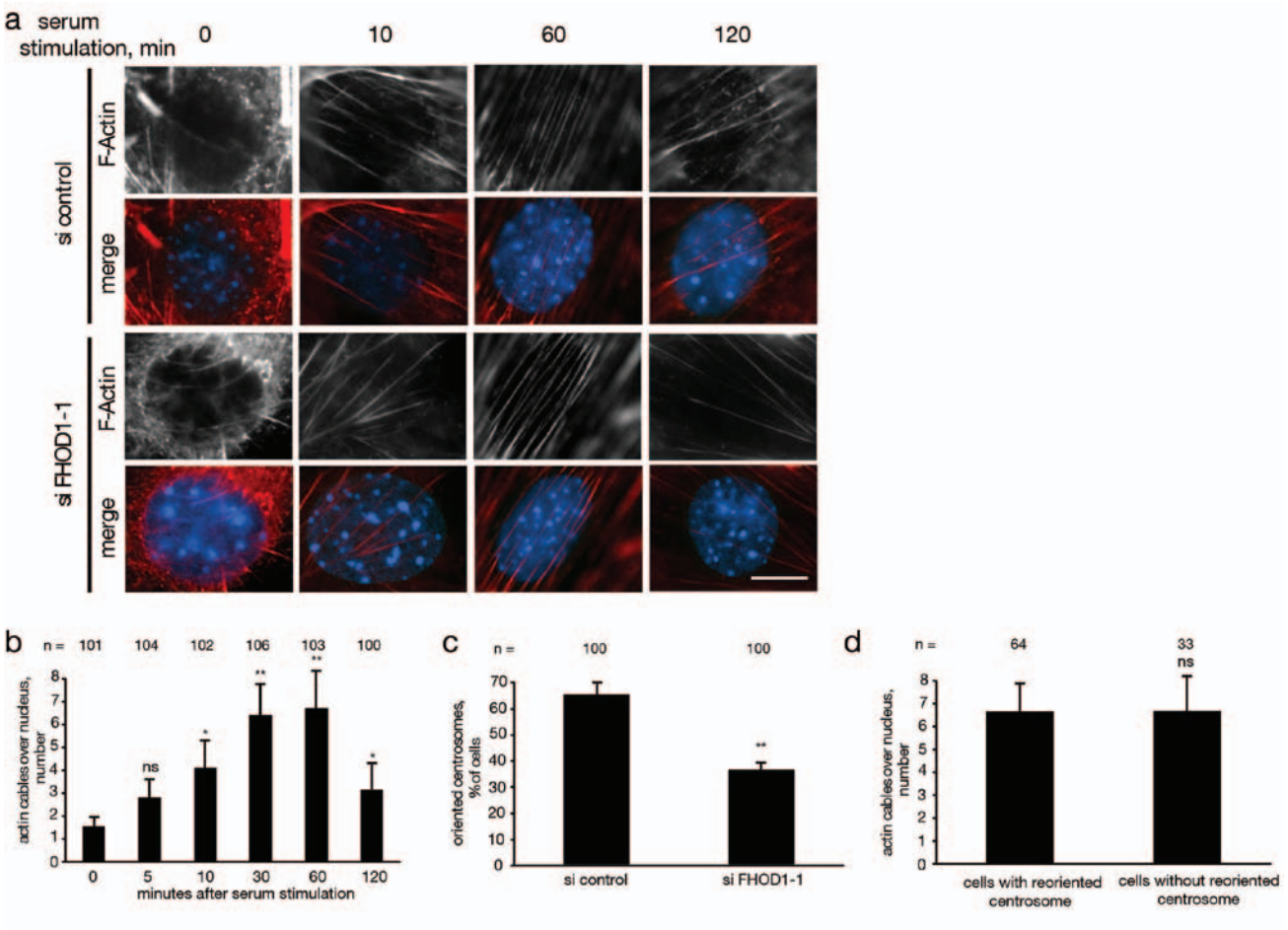

Supplementary Figure 3 FHOD1 knockdown does not affect actin structures induced by serum. Starved NIH3T3 fibroblasts were stimulated with 20 % FCS, fixed at indicated time points and stained with rhodamine phalloidin for F-actin (red) and DAPI for DNA (blue). (**a**) Fluorescence images of dorsal actin cables over the nucleus. Bar, 10 mm. (**b**) Quantification of the number of actin cables over the nucleus per cell in control siRNA cells at various time points after serum stimulation. (**c**) Quantification of centrosome orientation in serum-stimulated wound edge NIH3T3 fibroblasts. (**d**) Comparison of dorsal actin cables over nuclei in siFHOD1 treated cells with oriented and non-oriented centrosomes. Data in b-d are from 3 experiments; n = number of cells analysed per experiment is shown in (b, c, d). Error bars: SD. **, $P < 0.01$; *, $P < 0.05$; ns, not significantly different by two-tailed t-test.

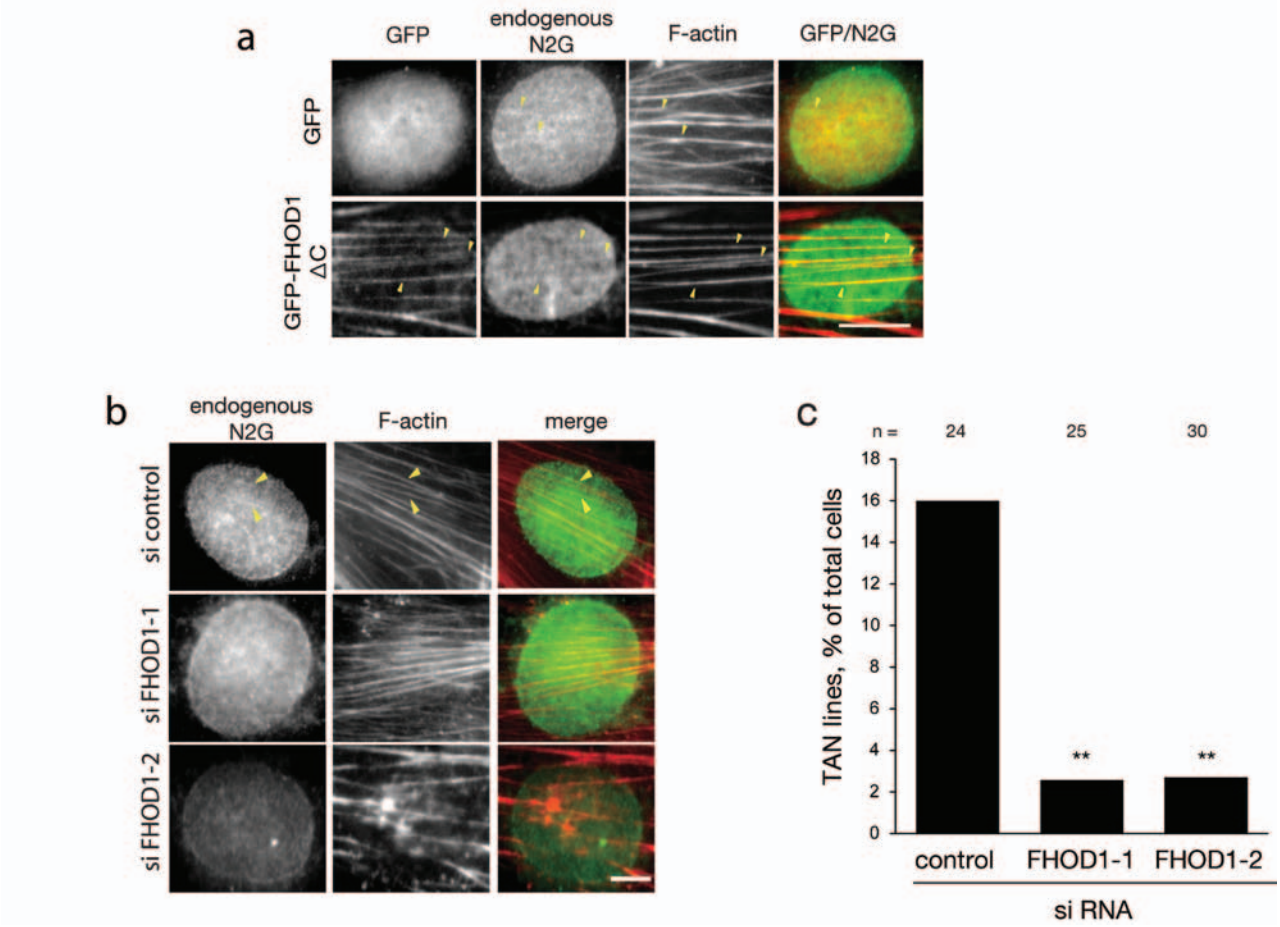

Supplementary Figure 4 Localization of FHOD1 ΔC with endogenous TAN lines and effect of FHOD1 knockdown on endogenous TAN lines. **(a)** Immunofluorescence images of GFP-FHOD1 ΔC and endogenous N2G on the dorsal surface of nuclei in LPA-stimulated NIH3T3 fibroblasts. Arrowheads, TAN lines containing N2G and dorsal actin cables and GFP-FHOD1 ΔC (bottom panels). Leading edge of the cell is toward the top. . Bar, 10 mm. **(b)** Immunofluorescence images of endogenous N2G (N2G antibody-stained) and F-actin (rhodamine phalloidin) in NIH3T3 fibroblasts treated with the indicated siRNAs. Arrowheads, TAN lines containing N2G co-localized with dorsal actin cables in control siRNA- treated cells. TAN lines are not observed in FHOD1 siRNA-treated cells. Bar, 5 mm. **(c)** Quantification of endogenous TAN lines in control siRNA- and FHOD1 siRNA-treated cells. Data are from 3 experiments; n = number of cells analysed per experiment shown in (c). **, $P<0.01$ by Fisher's exact test.

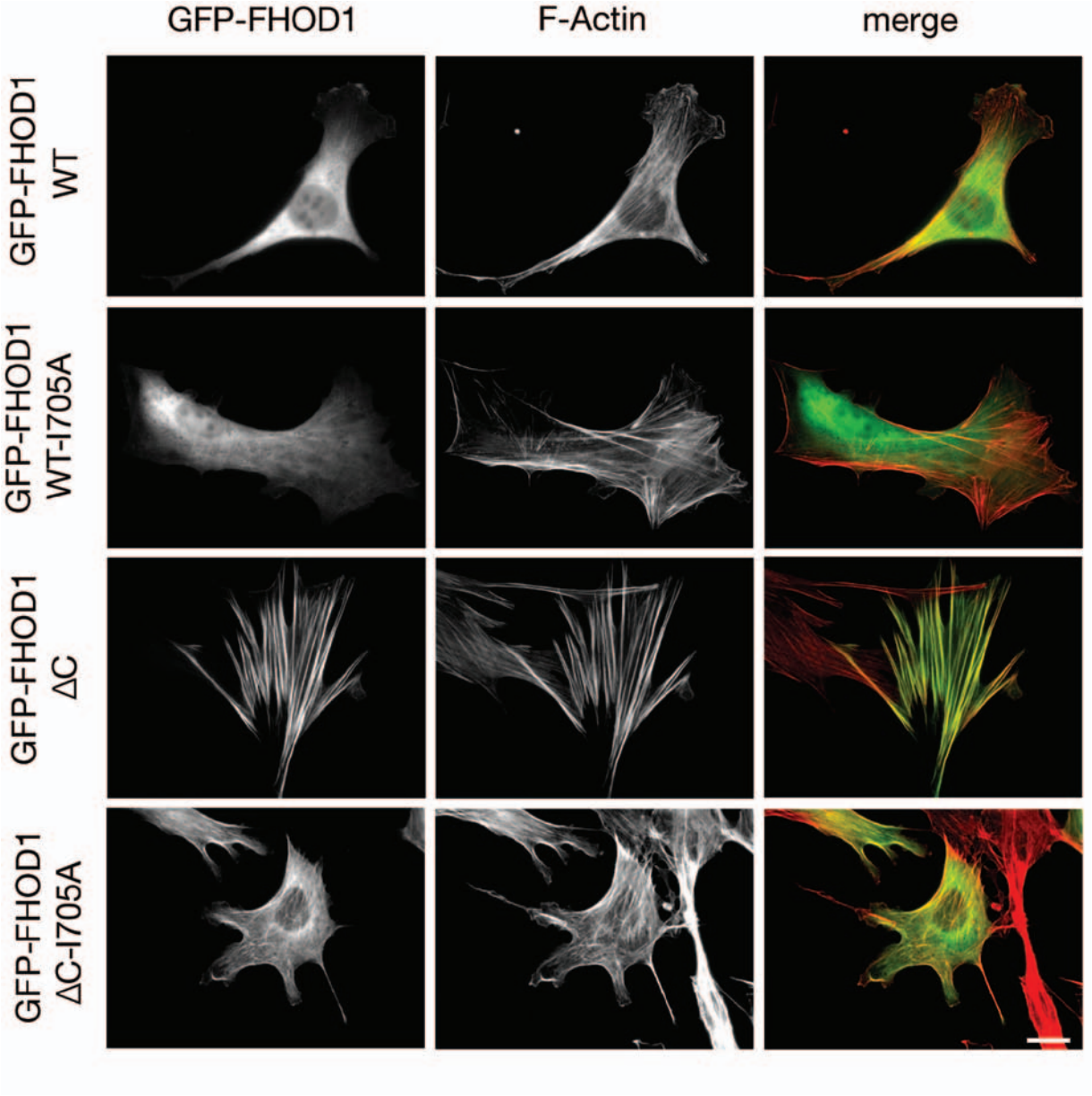

Supplementary Figure 5 The I705A mutation in active FHOD1 ΔC disrupts its induction of and localization with thick actin filament bundles. NIH3T3 cells expressing the indicated GFP-FHOD1 variants were stained for F-actin with rhodamine phalloidin. Note that active FHOD1 ΔC induces the formation of thick F-actin bundles associates with them. Actin bundle formation and actin filament association of FHOD1 is potently disrupted by the I705A mutation. Bar, 20 μm.

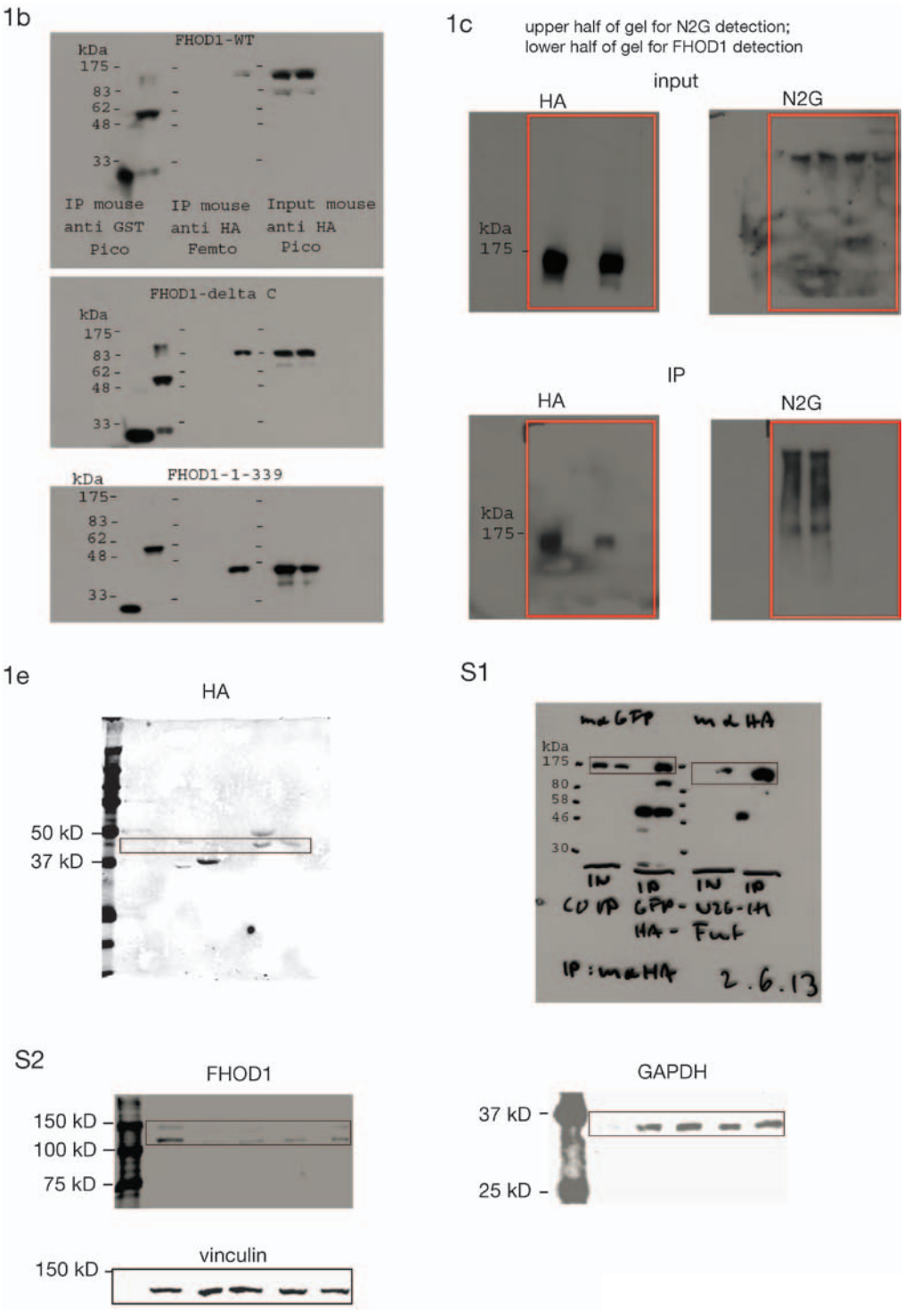

Supplementary Table 1 NIH3T3 sequence compared to mouse SYNE2 (NM_001005510)